RUB-TPII-05/96
February 1, 2008

Spontaneous annihilation of high-density matter in the electroweak theory

Jörg Schaldach[◇], Peter Sieber[◇], Dmitri Diakonov[*1], and Klaus Goeke[◇2]

[◇] *Inst. für Theor. Physik II, Ruhr-Universität Bochum, D-44780 Bochum, Germany*

[*] *St. Petersburg Nuclear Physics Institute, Gatchina, St.Petersburg 188350, Russia*

Abstract

In the presence of fermionic matter the topologically distinct vacua of the standard model are metastable and can decay by tunneling through the sphaleron barrier. This process annihilates one fermion per doublet due to the anomalous non-conservation of baryon and lepton currents and is accompanied by a production of gauge and Higgs bosons. We present a numerical method to obtain local bounce solutions which minimize the Euclidean action in the space of all configurations connecting two adjacent topological sectors. These solutions determine the decay rate and the configuration of the fields after the tunneling. We also follow the real time evolution of this configuration and analyze the spectrum of the created bosons. If the matter density exceeds some critical value, the exponentially suppressed tunneling triggers off an avalanche producing an enormous amount of bosons.

[1] diakonov@lnpi.spb.su

[2] goeke@hadron.tp2.ruhr-uni-bochum.de

1 Introduction

Baryon and lepton number violating processes in the electroweak theory have been the subject of many recent investigations. They are due to the anomaly of the baryon and lepton currents, discovered by 't Hooft [1], and the non-trivial topological structure of the electroweak theory. Faddeev [2] and Jackiw and Rebbi [3] found that the potential energy is periodic in a certain functional of the field, the Chern–Simons number $N_{\rm CS}$, so that instead of one unique vacuum there exist infinitely many field configurations with zero potential energy, classified by integer values of $N_{\rm CS}$.

Each transition between vacua with $\Delta N_{\rm CS} = 1$ is accompanied by a change of the baryon and lepton number by one unit per fermion generation. The vacua are separated by an energy barrier, called sphaleron barrier [4, 5], whose height is of the order of 10 TeV. Under ordinary conditions the barrier can only be overcome by tunneling, but the tunneling probability is suppressed by the factor $\exp(-2S_{\rm inst}) \approx 10^{-153}$ with the instanton action $S_{\rm inst} = 8\pi^2/g^2\,,\ g \approx 0.67$, which means that the process practically never happens.

Under special conditions, however, the fermion number violation rate might well be significant. For example, a large temperature (of the order of m_W) allows the system to cross the barrier classically [6, 7, 8]; this process might have played a key role for the generation and conservation of the baryon asymmetry in the early universe. The energy which is necessary to overcome the barrier can possibly also be provided by the incoming particles in a collision if the particle energy is of the order of $10 \sim 100$ TeV [9, 10, 11, 12]. Hence, fermion number violation might be observable at future supercolliders.

In this paper we will investigate a third possibility to obtain fermion number violation at a reasonable rate, namely in a surrounding of high density matter [13, 14]. The mechanism of how the suppression of the transition rate is reduced is as follows: Matter of high density is described by a chemical potential μ, which is, at temperature zero, the energy up to which the Fermi-levels are filled. A transition with $\Delta N_{\rm CS} = 1$ creates a fermion which has to be placed into the first free level, i.e. it has energy μ. This energy must be added to the potential energy of the gauge and Higgs bosons [13, 14]:

$$V^{\mu}_{\rm pot} = V_{\rm pot} + \mu N_{\rm CS}\ . \tag{1.1}$$

The extra term causes the previously degenerate vacua to become metastable and the height of the barrier to be reduced (see Fig. 1 where $V^{\mu}_{\rm pot}$ is plotted for

a negative μ) so that the tunneling probability increases. At a certain critical value $\mu_{\rm crit}$, the barrier disappears completely and the states at integer $N_{\rm CS}$ become unstable.

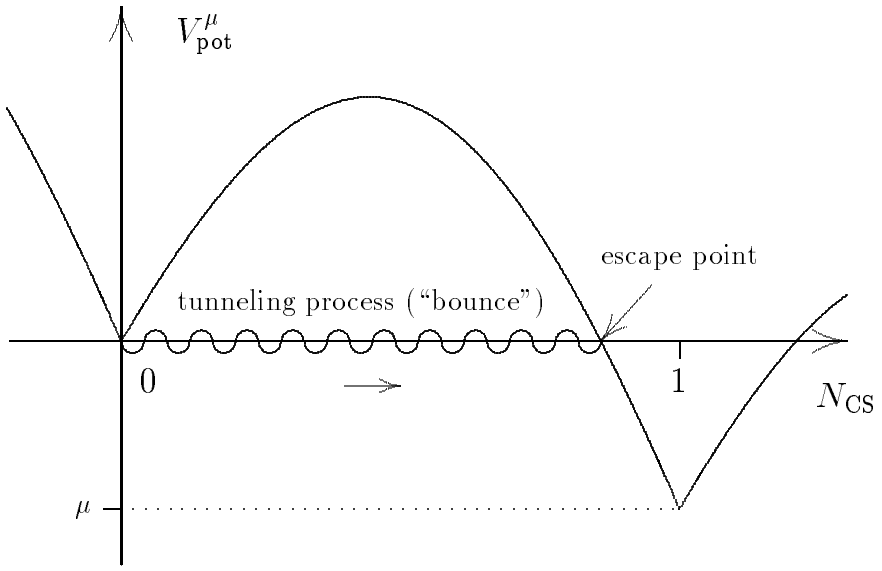

Fig. 1: Schematic plot of the tunneling process between two topological sectors.

The decay rate of a metastable state per volume can be calculated by the semi-classical WKB method. Following Coleman [15], it is expressed in the form $\Gamma/V = B\exp(-A)$. In order to find the exponent A one has to solve the classical Euclidean equations of motion, i.e. one has to find the classical motion of the system in the potential $-V^{\mu}_{\rm pot}$ from some metastable ground state (e.g. a state with $N_{\rm CS} = 0$, as indicated in Fig. 1) to a configuration with the same potential energy which is on the other side of the barrier. We call this configuration "escape point". The exponent A is twice the action of this motion, minimized over all possible escape points. In Euclidean space, after reaching the escape point the system would move back the same way to the original ground state, so that this process is called "the bounce" [15]. Hence, the bounce represents the minimum of the Euclidean action in the space of all possible paths from a metastable ground state to the other side of the barrier. The prefactor B basically contains zero mode factors and the determinant of small fluctuations about the bounce, but in this work we will not be concerned

with it and only compute the exponent A.

It turns out that the chemical potential (and hence the matter density) which is needed to obtain a reasonable decay rate is quite large, so that it can hardly occur under normal circumstances. Nevertheless, the results may still be relevant because the decay rate is closely related to the rate of baryon and lepton number violation at high particle energies [14]. Also, to our knowledge, this is the first investigation of the metastable vacuum decay in a real theory, beyond the so-called thin wall approximation; and since it is a hard technical problem, our numerical procedure might be useful in other applications, ranging from spontaneous decay of heavy nuclei to inflationary scenarios of the early universe.

In principle there are two different possibilities to find the bounce numerically: Either one solves the equations of motion by some initial value method like Runge–Kutta, or one considers the action as a functional of the fields and minimizes it in the space of all fields configurations. The first method seems to be unfeasible because the potential $-V^{\mu}_{\rm pot}$ has no lower bound so that a slight deviation from the correct path will cause the system to fall into some abyss of the potential $-V^{\mu}_{\rm pot}$. We have therefore decided to take the second route. For the numerical implementation of the minimization we use a discretization in space and time, based on a procedure presented by Adler and Piran [16], so that the action becomes a function of the values of the boson fields at the grid nodes. At each step one considers the action as a function of a certain field at a given point and keeps the other values fixed. A single step of a Newtonian algorithm is performed, then one takes another field or moves to the next point until one has performed a "sweep" through the whole lattice and starts with the next one.

Related problems have already been treated in the literature, for example in [17] the decay rate of a metastable state was also calculated by minimizing the Euclidean action on a grid in the context of technibaryons in the Skyrme model. In [18] the Euclidean action of the electroweak theory is minimized, but with respect to only a few parameters in the space of parametrized functions. A method how to minimize the action of a model with scalar fields was presented in [19]. A short letter about the present method has been published recently [20].

Another aim of this work is to investigate the fate of the system after the tunneling process has happened. It is known [15] that the motion in Euclidean

space does not only provide the probability of the barrier penetration, but also yields the most probable field configuration in which we will find the system after the tunneling. This is just the escape point of the bounce trajectory, i.e. the configuration at the other side of the barrier which belongs to the path in Euclidean space with the least action. The potential energy of the system after the tunneling is greater than the energy of the metastable minimum in its current topological sector (see Fig. 1). The difference $|\mu|$ is the energy of the annihilated fermion which is now at the disposal of the boson fields.

The field configuration then performs a real time motion in Minkowski space. Knowing the escape point field configuration and the field velocities (which are zero), one has to solve the standard Cauchi problem, which we perform by straightforward integration of the second-order differential equations. Usually the system will fall towards the minimum in the sector of the escape point, and eventually settles at that minimum. The original energy $|\mu|$ of fermions from the Fermi surface is converted into classical radiation of bosons. In 3+1 dimensions the amplitude of the outgoing wave package falls off as $1/t$ so that the generally nonlinear equations of motion can be linearized at large times t, and the outgoing fields take the form of spherical waves. In order to evaluate the particle content of the multi-boson final state one has to carry out a Fourier transformation of the fields after their amplitudes got small enough. At this point we basically follow the work of Hellmund and Kripfganz [21] (see also [22]), who took a slightly disturbed sphaleron as starting configuration, let it evolve in real time and analyzed the resulting multi-boson state. Our main modifications are the replacement of the sphaleron by the escape point of the bounce and the introduction of the chemical potential according to eq. (1.1).

In certain cases, however, when the fermion density is large enough though less than the critical density $\mu_{\rm crit}$, the real time evolution of the fields is utterly different. The fields will not quiet down at the minimum but "splash" over the *next* barrier leading to a still lower minimum (at $N_{\rm CS} = 2$ in Fig. 1), and so forth. As a result the fermion sea will be completely "dried out", and a huge amount of energy will be released in form of boson radiation. Naively, one would think that such an avalanche happens only when the fermion density exceeds the critical $\mu_{\rm crit}$ when the system is allowed to roll down classically. It is amusing that actually the avalanche-like fermion annihilation can be triggered off by a spontaneous tunneling process at the first stage.

The paper is organized as follows: In Section 2 we set up the model and

describe how matter of high density allows baryon and lepton number violating processes. In Section 3 we present in detail our numerical procedure to find the bounce trajectory. The classical motion after the tunneling is investigated in Section 4. In Section 5 we give the numerical results of our calculations, and finally we summarize our work in Section 6.

2 Decay of high–density matter by barrier penetration

We consider the minimal version of the standard electroweak theory with one Higgs doublet in the limit of vanishing Weinberg angle. We work with dimensionless rescaled quantities, the corresponding physical quantities can in general be obtained by multiplication with appropriate powers of the gauge boson mass m_W. Sometimes this factor is already included in the definition, for details see [8]. The bosonic part of the Lagrangian is

$$\mathcal{L} = \frac{m_W^4}{g^2}\left(-\tfrac{1}{4}F^a_{\mu\nu}F^{a\,\mu\nu} + \tfrac{1}{2}(D_\mu\Phi)^\dagger(D^\mu\Phi) - \tfrac{1}{32}\nu^2(\Phi^\dagger\Phi - 4)^2\right) \tag{2.1}$$

with the covariant derivative $D_\mu = \partial_\mu - iA_\mu\ ,\ A_\mu = \frac{1}{2}A^a_\mu\tau^a$, the field strength $F_{\mu\nu} = \frac{1}{2}F^a_{\mu\nu}\tau^a = i[D_\mu, D_\nu]\ ,\ F^a_{\mu\nu} = \partial_\mu A^a_\nu - \partial_\nu A^a_\mu + \epsilon^{abc}A^b_\mu A^c_\nu$, and the Higgs doublet $\Phi = \binom{\Phi^+}{\Phi^0}$. $\nu = m_H/m_W$ is the ratio of Higgs and gauge boson masses; the τ^a are the Pauli matrices. We work entirely in temporal gauge, $A_0 = 0$, which restricts possible gauge transformations to time-independent ones,

$$A_i \to U(A_i + i\partial_i)U^\dagger\ , \quad \Phi \to U\Phi \qquad \text{with} \qquad U = U(\mathbf{r}) \in SU(2)\ . \tag{2.2}$$

The potential and kinetic energy and the Chern–Simons index are

$$\begin{aligned} V_{\rm pot} &= \frac{m_W}{g^2}\int d^3\mathbf{r}\ \left[\tfrac{1}{4}(F^a_{ij})^2 + \tfrac{1}{2}(D_i\Phi)^\dagger(D_i\Phi) + \tfrac{1}{32}\nu^2(\Phi^\dagger\Phi - 4)^2\right]\ , \\ T_{\rm kin} &= \frac{m_W}{g^2}\int d^3\mathbf{r}\ \left[\tfrac{1}{2}(\dot A^a_i)^2 + \tfrac{1}{2}\dot\Phi^\dagger\dot\Phi\right]\ , \\ N_{\rm CS} &= \frac{1}{16\pi^2}\int d^3\mathbf{r}\ \left[\epsilon_{ijk}\left(A^a_i\partial_j A^a_k + \tfrac{1}{3}\epsilon_{abc}A^a_i A^b_j A^c_k\right)\right]\ . \end{aligned} \tag{2.3}$$

$N_{\rm CS}$ is only well-defined if the configuration space can be identified with the sphere S_3, which requires the fields to be continuous at infinity. We will always fix them to the trivial vacuum there ($A_i = 0,\ \Phi = \binom{0}{2}$). For vacuum configurations $A_i = iU\partial_i U^\dagger$ with $U \in SU(2)$ (pure gauge), $N_{\rm CS}$ is the integer winding

number of the mapping $S_3 \to SU(2) \sim S_3$. Adjacent topological sectors are separated by energy barriers. The field configurations which minimize the energy $V_{\rm pot}$ for given $N_{\rm CS}$ have been calculated numerically by Akiba, Kikuchi, and Yanagida (AKY) [23].

The fermions are coupled to the gauge and Higgs fields via the covariant derivative and the Yukawa coupling, respectively. We do not consider them explicitly, but note that due to the anomaly of the fermionic currents their number is not conserved, it varies with the Chern–Simons number of the classical bosonic fields. For each doublet (i) the fermion number changes as

$$\Delta N_i = \Delta N_{\rm CS} \; . \tag{2.4}$$

We assume to have a macroscopic amount of fermions of a very high density in thermal equilibrium at zero (or very low) temperature. There are $N_g(N_c+1) = 12$ doublets, three leptonic and nine quark ones. We describe them by the chemical potentials μ_i of the doublets; since we have zero temperature, μ_i is the energy up to which the fermionic levels are occupied (Fermi energy). In a process connecting two adjacent vacua one level crosses the gap, all others are shifted such that after the transition we have the same spectrum again. But now one more level is occupied or depleted, depending on whether the levels went up or down, hence the created or annihilated fermion has the energy μ_i. Eq. (2.4) allows to include the change of the fermionic energy into the bosonic energy functional. The new potential energy is [13, 14]

$$V_{\rm pot}^{\mu} = V_{\rm pot} + \mu N_{\rm CS} \tag{2.5}$$

with $V_{\rm pot}$ and $N_{\rm CS}$ from (2.3). $\mu = \sum_i \mu_i$ is the sum of the chemical potentials of the single doublets. Obviously, we have fixed the zero-point of the energy to the trivial vacuum with $N_{\rm CS} = 0$. Besides, we can neglect the change of the Fermi energy due to the creation or annihilation of a small number of fermions.

The additional term modifies the curvature of the potential around the ground states of the topological sectors. A calculation of the second derivative of $V_{\rm pot}^{\mu}$ with respect to the fields yields the following modes in momentum space [13, 14]:

$$1 + \mathbf{p}^2 \; , \qquad \nu^2 + \mathbf{p}^2 \; , \qquad \text{and} \qquad 1 + \mathbf{p}^2 \pm \frac{g^2 \mu}{8\pi^2 m_W} \, |\mathbf{p}| \; ; \tag{2.6}$$

besides, there is a zero mode due to gauge freedom. We see that there are

negative modes if $|\mu|$ exceeds the critical value

$$\mu_{\rm crit} = \frac{16\pi^2}{g^2}\, m_W \ . \tag{2.7}$$

Therefore, at $|\mu| > \mu_{\rm crit}$ the system may roll down classically without any tunneling. A numerical calculation [24] shows that indeed the minimal energy barriers between the topological sectors vanish in this case.

We are mainly interested in the case $0 < |\mu| < \mu_{\rm crit}$, where the topologically distinct minima with integer $N_{\rm CS}$ have different energies $V^{\mu}_{\rm pot} = \mu N_{\rm CS}$ and are separated by energy barriers. Therefore, they are only local minima and are thus metastable and can decay spontaneously by quantum tunneling to the adjacent topological sector with lower ground state energy. The energy difference $|\mu|$ between the two ground states is the energy of the bosonic fields after the tunneling that will eventually be carried away by the outgoing boson radiation.

As mentioned in the introduction, the tunneling rate per volume is of the form [15]

$$\Gamma/V = B \exp(-A) \tag{2.8}$$

where A is twice the Euclidean action of the bounce trajectory, which is the classical path that connects the decaying state and the turning point at the other side of the inverted barrier and minimizes this action. The prefactor B can be found from the small oscillation determinant about the bounce, with one negative mode and the zero modes removed. B also contains the Jacobian factors of the transformation groups which leave the action invariant, i.e. which correspond to the zero modes. The factors coming from translational invariance in space and time are not included in B but in the left hand side of (2.8), they lead to the transition *rate per volume*.

In this paper we concentrate on the calculation of A, we want to find the bounce solution numerically. This means to find classical fields $A^a_i(t,\mathbf{r})\,, \Phi(t,\mathbf{r})$ which represent a stationary point of the Euclidean action

$$S_E = \int_{-\infty}^{t_0} dt\, m_W^{-1}(T_{\rm kin} + V^{\mu}_{\rm pot}) \ . \tag{2.9}$$

At time $t = -\infty$ the fields form a metastable ground state with integer $N_{\rm CS}$ and $T_{\rm kin} = 0$; at $t = t_0$ the system reaches the turning point at the other side of the potential valley (which is — considering the tunneling process — the escape point at the other side of the barrier). Here again $T_{\rm kin} = 0$,

and $N_{\rm CS}$ takes a non-integer value belonging to the next topological sector. The bounce lasts infinitely long because it starts from a ground state with $\delta V^\mu_{\rm pot}/\delta A^a_i = \delta V^\mu_{\rm pot}/\delta\Phi = 0$. Consequently, t_0 is arbitrary, this corresponds to the translational invariance in time mentioned above.

As discussed previously, the choice of the temporal gauge still leaves the freedom of time independent transformations. Now we fix the gauge completely by demanding that at $t = -\infty$ the fields start from the trivial vacuum $A^a_i = 0$, $\Phi = \binom{0}{2}$ with $N_{\rm CS} = 0$ (and hence $V^\mu_{\rm pot} = T_{\rm kin} = 0$). Besides, we choose $\mu < 0$ so that the bounce moves from $N_{\rm CS} = 0$ to the topological sector with $N_{\rm CS} = 1$.

So far, we deal with 13 real functions depending on time t and space $\mathbf{r}$, nine from the gauge field A^a_i and four from the complex Higgs doublet Φ. But we expect that our bounce solution possesses higher symmetries than completely arbitrary fields. Therefore we restrict our ansatz to fields having the spherical symmetry of the sphaleron and the AKY configurations, which describe the minimal energy barrier:

$$\begin{aligned} A^a_i(t,\mathbf{r}) &= \epsilon_{aij} n_j \frac{1-A(t,r)}{r} + (\delta_{ai} - n_a n_i)\frac{B(t,r)}{r} + n_a n_i \frac{C(t,r)}{r}\,, \\ \Phi(t,\mathbf{r}) &= \Big[H(t,r) + iG(t,r)\,\mathbf{n}\cdot\boldsymbol{\varnothing}\Big]\begin{pmatrix}0\\2\end{pmatrix} \end{aligned} \tag{2.10}$$

with $r = |\mathbf{r}|$, $\mathbf{n} = \mathbf{r}/r$. This reduces the effort to five real functions depending on t and r. The free choice of the origin corresponds to the spatial translational invariance discussed after eq. (2.8). Gauge transformations within this ansatz are given by

$$U(r) = \exp\Big[\mathbf{n}\cdot\boldsymbol{\varnothing}\, iP(r)\Big]\,, \tag{2.11}$$

they transform the fields as

$$\begin{aligned} A(t,r) &\to A(t,r)\cos 2P(r) - B(t,r)\sin 2P(r)\,, \\ B(t,r) &\to B(t,r)\cos 2P(r) + A(t,r)\sin 2P(r)\,, \\ C(t,r) &\to C(t,r) + 2rP'(r)\,, \\ H(t,r) &\to H(t,r)\cos P(r) - G(t,r)\sin P(r)\,, \\ G(t,r) &\to G(t,r)\cos P(r) + H(t,r)\sin P(r)\,. \end{aligned} \tag{2.12}$$

We will use this transformation later to adjust the numerical solutions to our choice of the gauge.

As mentioned above, we choose a gauge which yields the trivial vacuum at $t = -\infty$. In this gauge the fields A_i^a, Φ of the bounce solution are continuous and differentiable everywhere and have finite potential and kinetic energy, because this is true for our starting point and will not be changed during the evolution governed by the Euclidean equations of motion. This requires the following behavior of the radial functions at $r = 0$:

$$\begin{aligned} A(t,r) &= 1 + a_2(t)\, r^2 + \mathcal{O}(r^3)\,, \\ B(t,r) &= b_1(t)\, r + \mathcal{O}(r^3)\,, \\ C(t,r) &= b_1(t)\, r + \mathcal{O}(r^3)\,, \\ H(t,r) &= h_0(t) + h_2(t)\, r^2 + \mathcal{O}(r^3)\,, \\ G(t,r) &= g_1(t)\, r + g_2(t)\, r^2 + \mathcal{O}(r^3)\,. \end{aligned} \tag{2.13}$$

The numerical determination of the bounce is performed by finding a stationary point of the Euclidean action directly, without using the equations of motion. In our spherical ansatz (2.10), S_E is a functional of the five functions A, B, C, H, G of eq. (2.10), depending on radial distance r and time t. The bounce has infinite extension as well in space as in time, but we can introduce new variables x and u which cover only finite intervals, for example

$$r(x) = \lambda_r \arctan\left(\tfrac{\pi}{2}\, x\right) \qquad \text{and} \qquad t(u) = \lambda_t \arctan\left(\tfrac{\pi}{2}\, u\right)\ , \tag{2.14}$$

and new profile functions depending on x and u. Using ansatz (2.10) and the substitution (2.14) we get

$$\begin{aligned} S_E \;=\; & \frac{S_{\text{inst}}}{2\pi} \int_{-1}^{u_0} du \int_0^1 dx\, \frac{1}{\omega\varphi} \Big[\omega^2 \Big(\dot{A}^2 + \dot{B}^2 + \tfrac{\dot{C}^2}{2} + 2r^2(\dot{H}^2 + \dot{G}^2) \Big) \\ & + \Big(\varphi A' + \tfrac{BC}{r} \Big)^2 + \Big(\varphi B' - \tfrac{AC}{r} \Big)^2 + 2r^2 \Big(\varphi H' + \tfrac{GC}{2r} \Big)^2 \\ & + 2r^2 \Big(\varphi G' - \tfrac{HC}{2r} \Big)^2 + \tfrac{1}{2r^2} (A^2 + B^2 - 1)^2 + H^2 \Big((A-1)^2 + B^2 \Big) \\ & + G^2 \Big((A+1)^2 + B^2 \Big) - 4BGH + \tfrac{1}{2} \nu^2 r^2 (H^2 + G^2 - 1)^2 \\ & + 2\rho \Big(\tfrac{C}{r} (A^2 + B^2 - 1) + \varphi B A' - \varphi (A-1) B' \Big) \Big] \end{aligned} \tag{2.15}$$

with

$$\rho = \frac{\mu}{\mu_{\text{crit}}}\ , \qquad \varphi = \varphi(x) = \left(\frac{dr}{dx} \right)^{-1}\ , \qquad \omega = \omega(u) = \left(\frac{dt}{du} \right)^{-1}\ , \tag{2.16}$$

and the dot and prime mean $\frac{d}{du}$ and $\frac{d}{dx}$, respectively. In the next section we describe how we find stationary points of the functional (2.15) numerically.

3 Numerical determination of the bounce trajectory

Our way to find a stationary point of S_E is the use of a relaxation method which was discussed by Adler and Piran in great detail [16]. The functional (2.15) is put on a two-dimensional grid of size $(n_u + 1) \times (n_x + 1)$. We distinguish the full node grid with points

$$(u_i,\, x_j) = (u_{\min} + i\,\Delta u,\, x_{\min} + j\,\Delta x)\;, \qquad \begin{pmatrix} i = 0, \ldots, n_u \\ j = 0, \ldots, n_x \end{pmatrix} \tag{3.1}$$

and the half node grid with points

$$(u_{i+\frac{1}{2}},\, x_{j+\frac{1}{2}}) = (u_{\min} + (i+\tfrac{1}{2})\,\Delta u,\, x_{\min} + (j+\tfrac{1}{2})\,\Delta x)\;, \quad \begin{pmatrix} i = 0, \ldots, n_u - 1 \\ j = 0, \ldots, n_x - 1 \end{pmatrix} \tag{3.2}$$

with

$$\Delta u = \frac{u_{\max} - u_{\min}}{n_u} \qquad \text{and} \qquad \Delta x = \frac{x_{\max} - x_{\min}}{n_x}\;. \tag{3.3}$$

For the substitution (2.14) the values are e.g. $u_{\min} = -1\,,\ u_{\max} = 0$ (for $t_0 = 0$), $x_{\min} = 0\,,\ x_{\max} = 1\,$. The five profile functions are put on the full node grid, the radial distance r and the derivatives ω and φ on the half node grid. We introduce the notation

$$A^i_j = A(u_i, x_j)\;, \qquad r_{j+\frac{1}{2}} = r(x_{j+\frac{1}{2}}) \tag{3.4}$$

and accordingly for the other functions. The use of the half node grid prevents the calculation of expressions like r or $1/r$ at the boundaries $r = \infty, 0$.

There are many different ways to put an integral as (2.15) on a grid, so that in the limit $n_u, n_x \to \infty$ the original functional is restored again. Therefore it is rather important to choose a discretization that is suitable for numerical treatment. Basically, we followed the suggestions of [16] here, but to fix the details we had to try and compare different ansatzes. For example, the property of some terms to vanish at the origin and cancel the $1/r$ divergence must not be lost by the discretization. It showed that terms as $(\varphi A' + \frac{BC}{r})$ should be discretized before being squared, and that instead of $C(t, r)$ the function

$$D(u, x) \equiv \frac{C(u, x)}{r(x)} \tag{3.5}$$

should be used, i.e. put on the full node grid as D^i_j. We use the following discretization for S_E, eq. (2.15), written here as sum over contributions from

grid cells centered at half node points $(u_{i+\frac{1}{2}},\, x_{j+\frac{1}{2}})$:

$$
\begin{aligned}
S_E^{\mathrm{grid}} = \frac{S_{\mathrm{inst}}}{2\pi} \sum_{i=0}^{n_u-1} \sum_{j=0}^{n_x-1} \frac{\Delta u\, \Delta x}{\omega_{i+\frac{1}{2}} \varphi_{j+\frac{1}{2}}} \Bigg[& \frac{\omega_{i+\frac{1}{2}}^2}{2\Delta u^2} \Big((A_j^{i+1} - A_j^i)^2 \\
& + (A_{j+1}^{i+1} - A_{j+1}^i)^2 + (B_j^{i+1} - B_j^i)^2 + (B_{j+1}^{i+1} - B_{j+1}^i)^2 \\
& + 2r_{j+\frac{1}{2}}^2 \Big((H_j^{i+1} - H_j^i)^2 + (H_{j+1}^{i+1} - H_{j+1}^i)^2 + (G_j^{i+1} - G_j^i)^2 \\
& + (G_{j+1}^{i+1} - G_{j+1}^i)^2 + \tfrac{1}{4}(D_j^{i+1} - D_j^i)^2 + \tfrac{1}{4}(D_{j+1}^{i+1} - D_{j+1}^i)^2 \Big) \Big) \\
+ \tfrac{1}{2} \Bigg\{ & \Big(\frac{\varphi_{j+\frac{1}{2}}}{\Delta x} (A_{j+1}^i - A_j^i) + \tfrac{1}{2}(B_j^i D_j^i + B_{j+1}^i D_{j+1}^i) \Big)^2 \\
& + \Big(\frac{\varphi_{j+\frac{1}{2}}}{\Delta x} (B_{j+1}^i - B_j^i) - \tfrac{1}{2}(A_j^i D_j^i + A_{j+1}^i D_{j+1}^i) \Big)^2 \\
& + 2r_{j+\frac{1}{2}}^2 \Big(\frac{\varphi_{j+\frac{1}{2}}}{\Delta x} (H_{j+1}^i - H_j^i) + \tfrac{1}{4}(G_j^i D_j^i + G_{j+1}^i D_{j+1}^i) \Big)^2 \\
& + 2r_{j+\frac{1}{2}}^2 \Big(\frac{\varphi_{j+\frac{1}{2}}}{\Delta x} (G_{j+1}^i - G_j^i) - \tfrac{1}{4}(H_j^i D_j^i + H_{j+1}^i D_{j+1}^i) \Big)^2 \\
& + \frac{1}{4r_{j+\frac{1}{2}}^2} \Big(({A_j^i}^2 + {B_j^i}^2 - 1)^2 + ({A_{j+1}^i}^2 + {B_{j+1}^i}^2 - 1)^2 \Big) \\
& + \tfrac{1}{2} \Big({H_j^i}^2 \Big((A_j^i - 1)^2 + {B_j^i}^2 \Big) + {H_{j+1}^i}^2 \Big((A_{j+1}^i - 1)^2 + {B_{j+1}^i}^2 \Big) \\
& \quad + {G_j^i}^2 \Big((A_j^i + 1)^2 + {B_j^i}^2 \Big) + {G_{j+1}^i}^2 \Big((A_{j+1}^i + 1)^2 + {B_{j+1}^i}^2 \Big) \\
& \quad - 4B_j^i G_j^i H_j^i - 4B_{j+1}^i G_{j+1}^i H_{j+1}^i \Big) \\
& + \tfrac{1}{4}\nu^2 r_{j+\frac{1}{2}}^2 \Big(({H_j^i}^2 + {G_j^i}^2 - 1)^2 + ({H_{j+1}^i}^2 + {G_{j+1}^i}^2 - 1)^2 \Big) \\
& + \rho \Big(D_j^i ({A_j^i}^2 + {B_j^i}^2 - 1) + D_{j+1}^i ({A_{j+1}^i}^2 + {B_{j+1}^i}^2 - 1) \Big) \\
& + \rho\, \frac{\varphi_{j+\frac{1}{2}}}{\Delta x} \Big((A_{j+1}^i - A_j^i)(B_j^i + B_{j+1}^i) - (A_j^i + A_{j+1}^i - 2)(B_{j+1}^i - B_j^i) \Big) \Bigg\} \\
+ \tfrac{1}{2} \Big\{ & \quad i \to i+1 \quad \Big\} \Bigg] .
\end{aligned}
\tag{3.6}
$$

Typically, we used grids of the size $n_u = n_x = 80$, in which case the profile functions are represented by $5 \cdot 81 \cdot 81 = 32805$ points. To find a stationary point of S_E^{grid} now means to find a configuration which fulfills the equations

$$
\frac{\partial S_E^{\mathrm{grid}}}{\partial A_j^i} = 0\,, \quad \frac{\partial S_E^{\mathrm{grid}}}{\partial B_j^i} = 0\,, \quad \frac{\partial S_E^{\mathrm{grid}}}{\partial D_j^i} = 0\,, \quad \frac{\partial S_E^{\mathrm{grid}}}{\partial H_j^i} = 0\,, \quad \frac{\partial S_E^{\mathrm{grid}}}{\partial G_j^i} = 0 \tag{3.7}
$$

for all i and j.

The solution is found iteratively until the configuration satisfies eq. (3.7) sufficiently well. In each step, only one single number A^i_j, B^i_j, D^i_j, H^i_j or G^i_j for certain i, j is changed, all others are held constant. "Sweeping" over the grid, we modify the field parameters one after another, where the order is only of minor importance. (We changed the five functions for given i, j and varied j for fixed i.) The change of e.g. A^i_j is governed only by the according equation $\partial S_E^{\rm grid}/\partial A^i_j = 0$, all other equations are not taken into account. We perform the first step of a Newtonian algorithm that would converge against the solution of that equation, i.e. we change the field parameter as

$$A^i_j \quad \longrightarrow \quad A^i_j - \kappa \, \frac{\partial S_E^{\rm grid}/\partial A^i_j}{\partial^2 S_E^{\rm grid}/\partial {A^i_j}^2} \,, \tag{3.8}$$

where in general for the damping parameter we choose $\kappa = 1$. The necessary partial derivatives in eq. (3.8) must be calculated from (3.6), we do not write them explicitly here.

Unfortunately, the bounce solution is not a local minimum, but only a saddle point of the Euclidean action: The problem is that because of the term $\mu N_{\rm CS}$ the Euclidean potential $-V^\mu_{\rm pot}$ is not bound from above, it can take positive values. Due to energy conservation the bounce itself between $N_{\rm CS} = 0$ and 1 cannot have positive potential energy $-V^\mu_{\rm pot}$ at any time, its total energy $E_{\rm tot} = T_{\rm kin} - V^\mu_{\rm pot}$ is constant and zero (Fig. 1). But in its vicinity, one can construct paths which have positive potential $-V^\mu_{\rm pot}$ for some time and which give a *lower* action than the bounce. We found that unrestricted sweeps according to (3.8) always lead to configurations of that kind. Once there, the system quickly evolves to enormously high winding numbers $N_{\rm CS}$ and an unlimitedly decreasing negative action. Thus, in order to avoid this instability, we have to prevent the system from acquiring positive potential $-V^\mu_{\rm pot}$. We did so by choosing an initial configuration with non-positive potential, and then rejecting all steps (3.8) which would yield a positive $-V^\mu_{\rm pot}$. If a step is not accepted, it is tried again with κ divided by 2; this is repeated up to five times before the step is completely rejected for the current sweep. Unfortunately, this method requires to calculate $V^\mu_{\rm pot}$ (or actually the change of $V^\mu_{\rm pot}$) for the current time slice after each single step, which slows down the algorithm considerably. There are more sophisticated ways to take into account invariances like energy conservation [19], but in our case the simple remedy proved to be the most effective. Within the restriction $-V^\mu_{\rm pot} \leq 0$ the bounce locally minimizes the action. Numerically,

we find indeed that the action decreases monotonically and converges to some limit.

As starting configuration we usually take an instanton-like configuration,

$$\begin{aligned} A(t,r) &= \cos\beta - 2\,\frac{rt\sin\beta + r^2\cos\beta}{r^2+t^2+\lambda^2}\,, \\ B(t,r) &= -\sin\beta - 2\,\frac{rt\cos\beta - r^2\sin\beta}{r^2+t^2+\lambda^2}\,, \\ D(t,r) &= -\frac{\lambda^2}{r(r^2+\lambda^2)}\Big(\beta + \frac{2rt}{r^2+t^2+\lambda^2}\Big)\,, \\ H(t,r) &= 1 - \tfrac{1}{2}\Big(1+\frac{t}{t^2+\lambda^2}\Big)\Big(1+\cos\frac{\pi r}{\sqrt{r^2+\lambda^2}}\Big)\,, \\ G(t,r) &= \tfrac{1}{2}\Big(1+\frac{t}{t^2+\lambda^2}\Big)\sin\frac{\pi r}{\sqrt{r^2+\lambda^2}}\,, \\ \text{with}\qquad \beta &= \beta(t,r) = \frac{2r}{\sqrt{r^2+\lambda^2}}\Big(\arctan\frac{t}{\sqrt{r^2+\lambda^2}} + \tfrac{\pi}{2}\Big)\,. \end{aligned} \tag{3.9}$$

The size parameter λ is chosen between 2 and 4. This configuration has potential $-V^\mu_{\rm pot} = 0$ at $t = -\infty$ and $-V^\mu_{\rm pot} = -\mu > 0$ at $t = \infty$; we choose the boundary $u_{\rm max}$ of the grid such that at $t(u_{\rm max})$ the potential crosses the zero line. Hence for $u_{\rm min} < u < u_{\rm max}$ we have $-V^\mu_{\rm pot} < 0$.

According to our gauge fixing and to eq. (2.13) the fields are fixed at some boundaries of our grid. For $u = u_{\rm min}$ ($t = -\infty$) or $x = x_{\rm max}$ ($r = \infty$) we have $A = H = 1\,,\ B = D = G = 0\,$, and for the origin $x = x_{\rm min}$ ($r = 0$) we know $A = 1\,,\ B = G = 0$. Accordingly, the following field parameters are held fixed:

$$\begin{aligned} A^0_j &= A^i_{n_x} = A^i_0 = 1\,, \\ B^0_j &= B^i_{n_x} = B^i_0 = 0\,, \\ G^0_j &= G^i_{n_x} = G^i_0 = 0\,, \\ D^0_j &= D^i_{n_x} = 0\,, \\ H^0_j &= H^i_{n_x} = 1\,. \end{aligned} \tag{3.10}$$

Unfortunately, if one only sweeps over the grid using (3.8), the outcome will not be a reasonable bounce solution, but a rather discontinuous and unusable configuration. Therefore the computational procedure cannot be run from start to end automatically, but requires the controlling and regulating of the user once in a while, which makes the work a tedious and long lasting one. The following problems arise:

The Euclidean action (2.15) contains no term $D' = \partial D/\partial x$. Hence, adjacent field parameters D^i_j and D^i_{j+1} are only weakly coupled and the D field easily

ceases to be smooth. Especially close to the origin the field is rather unstable, therefore we do not use (3.8) to fix D_0^i and D_1^i, but adjust them to a linear extrapolation through D_2^i and D_3^i. Nevertheless, in order to keep the fields reasonably smooth, we are forced to smooth them by an averaging procedure from time to time, where each field parameter is replaced by the average value of itself and some of its neighbors, with weight factors according to their distance. Certainly this disturbs the minimization algorithm and generally leads to a higher action again. But after some further sweeps the action is down to its earlier value again, and the fields are smoother now.

Another problem is the following: Close to $u = u_{\min}$ ($t = -\infty$) the factor $\omega = du/dt$ which governs the kinetic energy terms is rather small so that adjacent time slices are only weakly coupled. Therefore, the fact that we fixed the fields to the trivial vacuum at the $u = u_{\min}$ boundary hardly influences the configuration at larger times. Instead, we usually see that going from large u towards $u_{\min}$ the configuration continuously approaches a *non-trivial* vacuum state, and then close to $u_{\min}$ the fields show a discontinuous step from this non-trivial vacuum to the trivial one. We get rid of this step by performing a gauge transformation of the kind (2.12) which converts the non-trivial vacuum at the edge of the step to the trivial one. This gauge transformation is applied to all time slices except the ones close to $u_{\min}$ where the fields are already trivial.

Apart from the above manipulations which are necessary to keep the configuration in an acceptable shape, we also have the possibility to accelerate the convergence of the algorithm. The solution has to obey the energy conservation law $E_{\text{tot}} = T_{\text{kin}} - V_{\text{pot}}^{\mu} = 0$. Given some arbitrary configuration for which this is not the case, one can find a different time parameterization such that energy conservation is fulfilled. Practically, we leave the values $t(u_i)$ of the times at the grid nodes fixed and determine the fields of the reparametrized configuration at those times $t(u_i)$ by interpolation. By this operation one can gain a considerable decrease of the action without performing minimization sweeps.

Finally we remark that the grid size is not completely fixed, but it is adapted to the status of the minimization. Usually we start with a size of 41×41 nodes, and only when we are already close to the solution we double the grid to 81×81 points. Moreover, we observe that during the sweeps the bounce, especially its escape point where the potential reaches zero again, slowly moves towards smaller times. In principle, the time scale is arbitrary, as discussed above, but for numerical reasons a given configuration has slightly lower action when it is

shifted to smaller times. We find that the energy at a few points next to $u_{\max}$ becomes zero, so that the escape point does not longer coincide with $u_{\max}$. If the number of these points gets too large, we throw away the part of the configuration beyond the escape point, which results in a lower $u_{\max}$ and n_u. If n_u becomes too small, we double the grid in the time dimension only, i.e. we double n_u but leave n_x. For the final configuration we adjust the time scale such that the escape point is set on the origin, i.e. $t_0 = 0$.

Practically, the bounce trajectory is found by switching between the minimization sweeps and one of the manipulations described above. If any and which of the regulations should be performed has to be decided by looking at the actual field configuration. At first sight this procedure seems to be subjective and non-reproducible, but let us remark that before we stop the program, the last manipulation is always followed by at least 500 sweeps. Moreover we have always checked that the final configuration fulfills the equations of motion with excellent accuracy.

4 The real time evolution after the tunneling

In this section we show how we investigate the behavior of the boson field configuration after the barrier penetration and how we analyze the particle content of the state. We follow basically the procedure presented in [21], but instead of the sphaleron we take the escape point of the bounce as starting configuration.

The potential energy of the escape point is larger by $|\mu|$ than the potential energy of the ground state in the corresponding topological sector. Hence, the system performs a motion in the real time Minkowski space. The equations of motion within the spherical ansatz (2.10) are

$$\begin{aligned}
\ddot{A} &= \left(A' + \tfrac{BC}{r}\right)' - \tfrac{A}{r^2}(A^2 + B^2 - 1) + \left(\tfrac{C}{r} + 2\rho\right)\left(B' - \tfrac{AC}{r}\right) \\
&\qquad - A(H^2 + G^2) + H^2 - G^2\,, \\
\ddot{B} &= \left(B' - \tfrac{AC}{r}\right)' - \tfrac{B}{r^2}(A^2 + B^2 - 1) - \left(\tfrac{C}{r} + 2\rho\right)\left(A' + \tfrac{BC}{r}\right) \\
&\qquad - B(H^2 + G^2) + 2HG\,, \\
\ddot{C} &= \tfrac{2A}{r}\left(B' - \tfrac{AC}{r}\right) - \tfrac{2B}{r}\left(A' + \tfrac{BC}{r}\right) - C(H^2 + G^2) \\
&\qquad + 2r(HG' - H'G) - \tfrac{2\rho}{r}(A^2 + B^2 - 1)\,,
\end{aligned}$$

$$
\begin{aligned}
\ddot{H} &= \tfrac{1}{r}(rH)'' + \tfrac{1}{2r^2}(CG + C'Gr + 2CG'r) + \tfrac{1}{r^2}(AH + BG) \\
&\quad - \tfrac{H}{2r^2}\Big(1 + A^2 + B^2 + \tfrac{C^2}{2}\Big) - \tfrac{\nu^2}{2}H(H^2 + G^2 - 1)\,, \\
\ddot{G} &= \tfrac{1}{r}(rG)'' - \tfrac{1}{2r^2}(CH + C'Hr + 2CH'r) + \tfrac{1}{r^2}(BH - AG) \\
&\quad - \tfrac{G}{2r^2}\Big(1 + A^2 + B^2 + \tfrac{C^2}{2}\Big) - \tfrac{\nu^2}{2}G(H^2 + G^2 - 1)\,, \quad (4.1)
\end{aligned}
$$

where the dot means the derivative with respect to the time t and the prime with respect to the radial coordinate r.

These equations and the condition that at $t = 0$ the system starts at the escape point of the bounce with kinetic energy zero (i.e. $\dot{A}(0) = \dot{B}(0) = \dot{C}(0) = \dot{H}(0) = \dot{G}(0) = 0$) form a Cauchi problem which is solved by direct integration. To do this we discretize the Minkowskian action in the same way as the Euclidean action, which means we take eq. (3.6) and reverse the sign of the terms stemming from the potential energy. Moreover we identify $t(u) = u$ instead of eq. (2.14), so that $\omega(u) = 1$, but we still keep the relation between r and x of (2.14). We obtain discretized equations of motion by deriving the discretized Minkowskian action with respect to the field coordinates $A^i_j, \ldots, G^i_j$. These equations are solved for the variables $A^{i+1}_j, \ldots, G^{i+1}_j$ so that we obtain the fields with time index i+1 as a function of those with indices i and i–1. By iterative application of these equations it is then possible to evaluate the propagation of the system from the initial configuration at $t = 0$ to arbitrary positive times.

The grid of the discretization can be much more dense here than in the case of the Euclidean problem. Usually we take 800 steps per time unit and 3000 grid nodes in the interval from $x = 0$ to $x = 1$. We checked that the results are stable with respect to a further increase of these parameters. The total time how long we follow the propagation of the fields is typically around 20 to 30 (in units of m_W^{-1}).

As in the Euclidean case, special care has to be taken in order to treat the fields close to the origin $r = 0$ adequately. If the numerical solution does not exactly fulfill the expansion given by eq. (2.13), some terms of the r.h.s. of eq. (4.1) become singular. Hence, even a slight deviation from this expansion increases rather quickly with t and finally results in a strong divergence of the fields close to $r = 0$. Since small numerical errors will always cause this to happen we cannot take the discretized equations of motion close to the origin, but we rather impose the behavior of (2.13) by hand. For about the first 50 of the 3000 points we determine the fields not by the iteration method but by

eq. (2.13) where the coefficients $a_2(t)$ etc. are chosen such that the functions $A, \ldots, H$ are continuous and differentiable at the matching point between the numerical solution and the fit (2.13).

We find that for most sets of parameters ν and ρ after some time the fields perform small oscillations about some vacuum configuration $\bar{A}(r), \ldots, \bar{G}(r)$ in the topological sector of the escape point (which is the one with $N_{\mathrm{CS}} = 1$ for our choice of gauge). An indication for this behavior is that N_{CS}, V^{μ}_{pot}, and T_{kin} do not change any more with t, the energies take constant values $\pm\frac{|\mu|}{2}$ according to the virial theorem.

The Fourier analysis of the small oscillations is greatly simplified if the vacuum about which the fields are fluctuating is the trivial one. For this reason we perform a time independent gauge transformation of the type (2.12) which transforms the configuration $\bar{A}(r), \ldots, \bar{G}(r)$ into the trivial vacuum. In order to determine the configuration $\bar{A}(r), \ldots, \bar{G}(r)$, we start the propagation of the fields with the original escape point and average the fields:

$$\bar{A}(r) = \frac{1}{t - t_s} \int_{t_s}^{t} dt'\, A(t', r)\,, \tag{4.2}$$

and equivalently for the other profiles. t_s is some time where the system already performs small oscillations. We checked that $\bar{A}(r), \ldots, \bar{G}(r)$ are independent of t if t is large enough and that they in fact represent a vacuum configuration with $N_{\mathrm{CS}} = 1$.

The gauge transformation which transforms $\bar{A}(r), \ldots, \bar{G}(r)$ into the trivial vacuum changes the Chern–Simons number by $\Delta N_{\mathrm{CS}} = -1$. We apply it to our starting configuration, the escape point, which hereby gets a Chern–Simons number between -1 and 0 and the potential energy $V^{\mu}_{\mathrm{pot}} = |\mu|$. Now we start the propagation again with the starting configuration in the new gauge. By performing the same averaging process again, we can check that the system now indeed fluctuates about the trivial vacuum with excellent accuracy, which proves that the gauge invariance is correctly reproduced in our numerics.

For the following we assume that the system has reached the status where it can be described by small fluctuations about the trivial vacuum. We denote these fluctuations with small letters:

$$\begin{aligned} A(t,r) &= 1 + a(t,r)\,, \qquad & B(t,r) &= b(t,r)\,, \qquad & C(t,r) &= c(t,r)\,, \\ H(t,r) &= 1 + h(t,r)\,, \qquad & G(t,r) &= f(t,r)\,, \end{aligned} \tag{4.3}$$

and expand the energy to second order in the fluctuations:

$$\begin{aligned}
T^{(2)}_{\rm kin} &= \frac{4\pi m_W}{g^2}\int_0^\infty dr\left(\dot a^2+\dot b^2+\tfrac{\dot c^2}{2}+2r^2(\dot h^2+\dot f^2)\right),\\
V^{\mu\ (2)}_{\rm pot} &= \frac{4\pi m_W}{g^2}\int_0^\infty dr\left[\tfrac{2a^2}{r^2}+a'^2+\Big(b'-\tfrac{c}{r}\Big)^2+a^2+b^2+\tfrac{c^2}{2}+4f^2-4bf\right.\\
&\qquad\left.-2rcf'+2r^2(h'^2+f'^2)+2\nu^2r^2h^2+2\rho\Big(a'b-b'a+\tfrac{2ac}{r}\Big)\right],\\
E^{(2)}_{\rm tot} &= T^{(2)}_{\rm kin}+V^{\mu\ (2)}_{\rm pot}.
\end{aligned}\tag{4.4}$$

We found that $V^{\mu\ (2)}_{\rm pot}$ and $V^{\mu}_{\rm pot}$ coincide up to a deviation of less than 1% for large t which indicates that the system has perfectly linearized. The potential in second order leads to the linear equations of motion

$$\begin{aligned}
\ddot a &= a''-a\Big(1+\tfrac{2}{r^2}\Big)+2\rho\Big(b'-\tfrac{c}{r}\Big),\\
\ddot b &= \Big(b'-\tfrac{c}{r}\Big)'-b+2f-2\rho a',\\
\ddot c &= \tfrac{2}{r}\Big(b'-\tfrac{c}{r}\Big)-c+2rf'-4\rho\tfrac{a}{r},\\
r\ddot h &= (rh)''-\nu^2rh,\\
r\ddot f &= (rf)''-\tfrac{1}{2r}(rc)'+\tfrac{b}{r}-\tfrac{2f}{r}.
\end{aligned}\tag{4.5}$$

In the case $\rho\neq 0$, for an arbitrary fixed momentum k the solution is

$$\begin{aligned}
a_k(t,r) &= \frac{3}{2}\Big(\beta^k_1(t)-\beta^k_2(t)\Big)\,rj_1(kr),\\
b_k(t,r) &= \Big(\beta^k_0(t)+\beta^k_1(t)+\beta^k_2(t)+\zeta^k(t)\Big)\,rj_0(kr)\\
&\quad+\Big(\beta^k_0(t)-\tfrac{1}{2}\beta^k_1(t)-\tfrac{1}{2}\beta^k_2(t)+\zeta^k(t)\Big)\,rj_2(kr),\\
c_k(t,r) &= \Big(\beta^k_0(t)+\beta^k_1(t)+\beta^k_2(t)+\zeta^k(t)\Big)\,rj_0(kr)\\
&\quad-2\Big(\beta^k_0(t)-\tfrac{1}{2}\beta^k_1(t)-\tfrac{1}{2}\beta^k_2(t)+\zeta^k(t)\Big)\,rj_2(kr),\\
h_k(t,r) &= \gamma^k(t)\,j_0(kr),\\
f_k(t,r) &= -\frac{3}{2}\Big(k\beta^k_0(t)-\tfrac{1}{k}\zeta^k(t)\Big)\,j_1(kr)
\end{aligned}\tag{4.6}$$

with

$$\beta^k_i(t)=\beta_i(k)\sin(\omega_it+\alpha_i),\ i=0,1,2,\quad \gamma^k(t)=\gamma(k)\sin(\Omega t+\delta),\quad \zeta^k(t)=c_1t+c_2,$$

$$\omega_0^2=k^2+1,\quad \omega_{1,2}^2=k^2+1\pm 2k\rho,\quad \Omega^2=k^2+\nu^2,\tag{4.7}$$

and $j_i(kr)$ are the spherical Bessel functions. The phase shifts α_i, δ and the c_i are fixed constants depending on the initial conditions. The zero mode in eq. (4.6) is due to the gauge freedom; since we have fixed the gauge its amplitude

$\zeta^k(t)$ is zero. The frequencies ω_i, $i = 0, 1, 2$ are eigenmodes of free gauge bosons (in dimensionful units 1 has to be replaced by m_W^2 in eq. (4.7)), Ω represents the free Higgs particle eigenstates.

The coefficients can be evaluated by Fourier transformation:

$$\begin{aligned}
\gamma^k(t) &= \tfrac{2k^2}{\pi} \int_0^\infty dr\, r^2 j_0(kr)\,(H(t,r)-1)\,, \qquad (4.8)\\
\beta_0^k(t) &= -\tfrac{4k}{3\pi} \int_0^\infty dr\, r^2 j_1(kr)\, G(t,r)\\
&= \tfrac{2k^2}{9\pi} \int_0^\infty dr\, r \Big[j_0(kr)\,(2B(t,r)+C(t,r))\\
&\qquad\qquad + j_2(kr)\,(2B(t,r)-2C(t,r)) \Big]\,,\\
\beta_{1,2}^k(t) &= \tfrac{2k^2}{9\pi} \int_0^\infty dr\, r \Big[j_0(kr)\,(2B(t,r)+C(t,r))\\
&\qquad\qquad - j_2(kr)\,(B(t,r)-C(t,r)) \pm 3 j_1(kr)\,(A(t,r)-1) \Big]\,.
\end{aligned}$$

To find the amplitudes $\beta_i(k)$, $\gamma(k)$ we Fourier transform the numerical solution of the equations of motion (4.1) according to eq. (4.8). The resulting functions $\beta_i^k(t)$, $\gamma^k(t)$ should oscillate according to eq. (4.7) when the system has settled to small fluctuations about the vacuum. This is the case after some time $t_{\rm osc}$ (typically $\sim 15\, m_W^{-1}$) with excellent accuracy. Moreover we checked that the two different formulas for $\beta_0^k(t)$ in eq. (4.8) numerically lead to the same result. Fitting the functions $\beta_i^k(t)$, $\gamma^k(t)$ for $t > t_{\rm osc}$ with the corresponding $\sin(\omega_i t + \alpha_i)$, $\sin(\Omega t + \delta)$ of eq. (4.7) yields the amplitudes $\beta_i(k)$, $\gamma(k)$.

One obtains for the total energy of the linearized system in momentum space (its coordinate space representation is given by eq. (4.4); the numerical values coincide up to a deviation of less than 2%):

$$\begin{aligned}
E_{\rm tot}^{(2)} &= E_W + E_H = m_W \int_0^\infty dk\, e_W(k) + m_W \int_0^\infty dk\, e_H(k)\\
&= \frac{9\pi^2 m_W}{g^2} \int_0^\infty \frac{dk}{k^2} \Big(\omega_0^4(k)\beta_0^2(k) + \omega_1^2(k)\beta_1^2(k) + \omega_2^2(k)\beta_2^2(k) \Big)\\
&\quad + \frac{4\pi^2 m_W}{g^2} \int_0^\infty \frac{dk}{k^2}\, \Omega^2(k)\gamma^2(k)\,. \qquad (4.9)
\end{aligned}$$

Since energy and particle density are related by $e(k) = \omega(k) n(k)$ we can extract the total number of particles:

$$\begin{aligned}
N_W &= \frac{9\pi^2}{g^2} \int_0^\infty \frac{dk}{k^2} \Big(\omega_0^3(k)\beta_0^2(k) + \omega_1(k)\beta_1^2(k) + \omega_2(k)\beta_2^2(k) \Big)\,,\\
N_H &= \frac{4\pi^2}{g^2} \int_0^\infty \frac{dk}{k^2}\, \Omega(k)\gamma^2(k)\,. \qquad (4.10)
\end{aligned}$$

5 Results

In this section we present the numerical results of our calculation. Our model contains two free parameters, the Higgs mass $\nu = m_H/m_W$ and the chemical potential $\rho = \mu/\mu_{\rm crit}$. We performed the calculations for the values $\nu = 0$, 1, 10, and $\rho = -0.2$, -0.4, -0.6, and -0.8. Moreover we investigated the case $\nu = 1$, $\rho = -0.9$. The values for ν cover a wide range of Higgs masses, but it turns out that most results do not depend too much on ν. The choice $\nu = 0$ is certainly not physical since essential features of the model, like spontaneous symmetry breaking, disappear. It should therefore be understood as limiting case of small masses. In fact we found that the configurations obtained for $\nu = 0$ and a mass like $\nu = 0.1$ are almost identical. Similarly $\nu = 10$ is an example for a large Higgs mass.

5.1 Barrier penetration

In Fig. 2 we show the potential and kinetic energy as well as the Chern–Simons number as functions of the time for the bounce trajectories with chemical potentials $\rho = -0.2$ and -0.8 and the Higgs mass $\nu = 1$. The arbitrariness of the time scale has been removed by setting the time when the system reaches the escape point at the other side of the barrier to $t = 0$. It can be seen that the energy conservation law $E_{\rm tot} = T_{\rm kin} - V^{\mu}_{\rm pot} \equiv 0$ is excellently fulfilled. For $\rho = -0.8$ the energies $T_{\rm kin}$ and $V^{\mu}_{\rm pot}$ are much smaller than for $\rho = -0.2$. Also the value of $N_{\rm CS}$ at $t = 0$ is lower in the case $\rho = -0.8$. The reason for this behavior is that the barrier between the trivial vacuum and the topological sector with $N_{\rm CS} = 1$ decreases if $|\rho|$ is increased so that less action is necessary to penetrate it and the system can escape at a configuration with lower winding number $N_{\rm CS}$. The extension of the bounce in time (and also in space, see below), however, increases with $|\rho|$. For example, in the case $\rho = -0.2$ the system moves out of the trivial vacuum significantly at about $t \approx -2$ while this happens for $\rho = -0.8$ already at about $t \approx -4$. The Chern–Simons term in the functional S_E (eq. (2.15)) lowers the action for large sizes, and its influence becomes stronger with increasing $|\rho|$. Hence for large $|\rho|$ configurations with large sizes are favored, while for low $|\rho|$ the minimum is taken at a field configuration with a small size. In the limit $\rho \to 0$ one would even obtain a configuration with size zero (see below).

The field configuration at the escape point of the bounce trajectory at $t = 0$

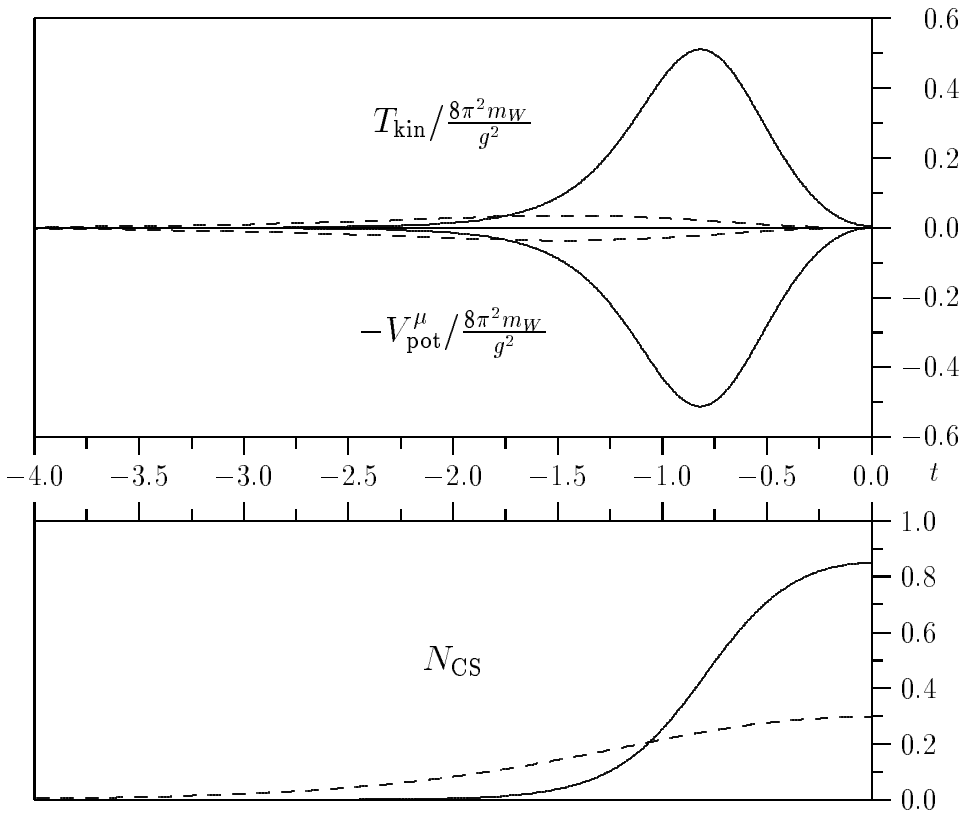

Fig. 2: The potential energy $-V^{\mu}_{\rm pot}$, the kinetic energy $T_{\rm kin}$, and the Chern–Simons number $N_{\rm CS}$ versus time t (in units of m_W^{-1}) for chemical potentials $\rho = \mu/\mu_{\rm crit} = -0.2$ (solid lines) and -0.8 (dashed lines). The Higgs mass is $\nu = m_H/m_W = 1$.

is interesting by itself, since subsequent calculations like the investigation of the real time behavior of the system require only this configuration rather than the complete bounce trajectory. In Fig. 3 we have plotted the profile functions at $t = 0$ again for the two cases $\rho = -0.2$ and -0.8, and the Higgs mass $\nu = 1$. What we saw in Fig. 2 for the time t, we find here for the space coordinate r: The deviation of the fields from their values in the trivial vacuum is much stronger for $\rho = -0.2$, but the region where they deviate is less extended. A suitable and accurate analytic fit for the configurations at the escape point is provided in the appendix.

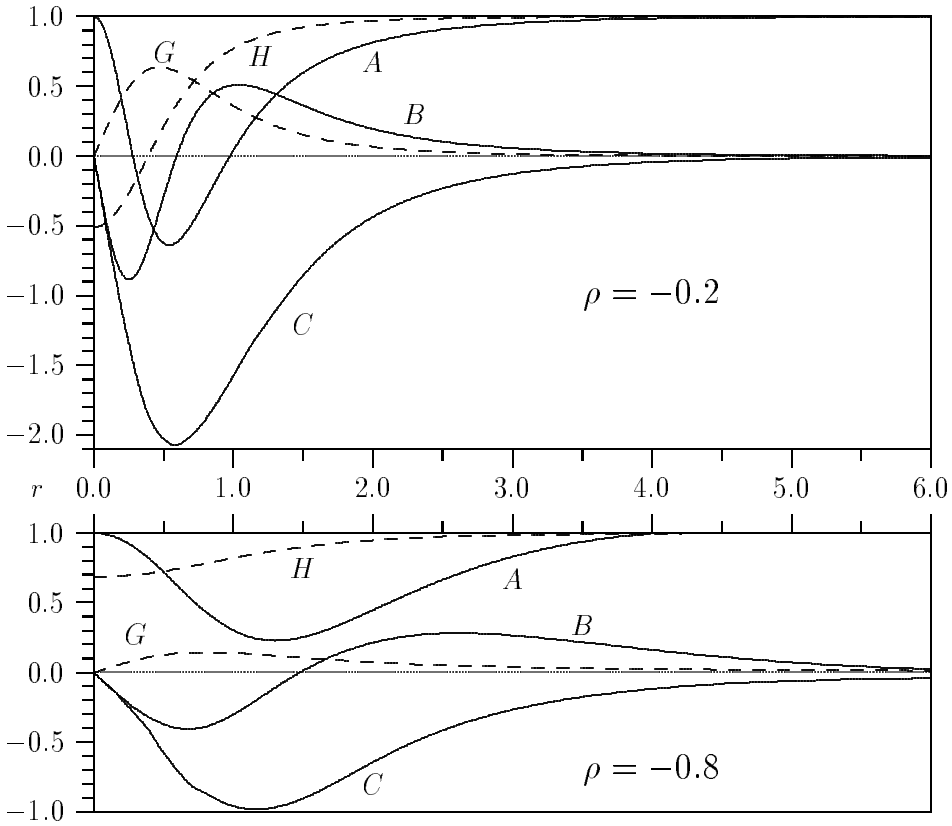

Fig. 3: The profile functions A, B, C (solid lines), and H and G (dashed lines) versus the radial distance r (in units of m_W^{-1}) of the configuration at the escape point of the bounce trajectory for $\rho = \mu/\mu_{\rm crit} = -0.2$ and $\rho = -0.8$, and the Higgs mass $\nu = m_H/m_W = 1$.

	$\rho = \mu/\mu_{\rm crit}$					
$\nu = \frac{m_H}{m_W}$	0.0	−0.2	−0.4	−0.6	−0.8	−1.0
0	1.00[1)]	0.81	0.54	0.30	0.11	0.00[1)]
1	1.00[1)]	0.82	0.58	0.34	0.14	0.00[1)]
10	1.00[1)]	0.86	0.66	0.45	0.19	0.00[1)]

[1)] known from theory

Tab. 1: The action $S_E/S_{\rm inst}$ of the bounce trajectory for various values of the chemical potential ρ and the Higgs mass ν.

	$\rho = \mu/\mu_{\rm crit}$					
$\nu = \frac{m_H}{m_W}$	0.0	-0.2	-0.4	-0.6	-0.8	-1.0
0	1.00[1)]	0.83/0.85[2)]	0.64/0.66[2)]	0.44/0.47[2)]	0.22/0.24[2)]	0.00[1)]
1	1.00[1)]	0.85	0.68	0.51	0.30	0.00[1)]
10	1.00[1)]	0.87	0.74	0.66	0.42/0.42[2)]	0.00[1)]

[1)] known from theory

[2)] results of two different trajectories with the same action

Tab. 2: The Chern–Simons number $N_{\rm CS}^{\rm esc}$ of the escape point of the bounce trajectory for various values of the chemical potential ρ and the Higgs mass ν.

In Table 1 we give the results for the action S_E of the tunneling process in units of the action $S_{\rm inst} = \frac{8\pi^2}{g^2}$ of the instanton in pure gauge theory. In Table 2 we show the Chern–Simons number $N_{\rm CS}^{\rm esc}$ of the configuration at the escape point. For $\rho = -1$ the barrier vanishes so that the tunneling process is reduced to a single point in the configuration space, namely the trivial vacuum. Hence in this case the action and $N_{\rm CS}^{\rm esc}$ are both 0. For $\rho \to 0$ the field configuration which minimizes the action tends to an instanton with size zero, so that the bounce action equals the instanton action and the configuration at the escape point is a vacuum with $N_{\rm CS} = 1$. In a pure gauge field theory the solution for $\rho = 0$ would be an instanton of arbitrary size, but here the scale invariance is destroyed by the non-zero vacuum expectation value of the Higgs field, so that for a finite size the action would be larger than the instanton action [25]. Hence in the limit $\rho \to 0$ we obtain a trajectory with size zero. For $-1 < \rho < 0$, however, due to the Chern–Simons term the minimum of the action is taken by a configuration with finite size. The accuracy of the data in Tables 1 and 2 can be estimated by increasing the density of the lattice (which is usually of size about 81×81) and the number of sweeps (usually of the order of 10000). We find that the numerical error of the results is around 1%. For each set of parameters ν, ρ we performed two independent minimizations, starting from two rather different field configurations like e.g. instantons with size $\lambda = 2$ and $\lambda = 4$ (see eq. (3.9)). For $\nu = 1$, both minimizations always ran towards the same bounce trajectory, within the given frame of accuracy. For $\nu = 0$ and $\nu = 10$, however, the two minimizations sometimes produced different trajectories, which have the same action, but different $N_{\rm CS}^{\rm esc}$, and also different behavior of the functions $V_{\rm pot}^{\mu}(t)$,

$N_{\rm CS}(t)$. Using a suitable averaging procedure, one finds that there exists an infinite number of different paths, which all have the same action (up to a deviation of 1%). Two conclusions are possible: Either the bounce trajectory is not unique, i.e the action has a zero mode, or there is a unique, but very shallow minimum.

Unfortunately, the numerical accuracy of our method does not allow to distinguish between those two possibilities, but for the following investigations this is quite irrelevant, anyway: In the case of a true zero mode the different tunneling trajectories will be taken with *exactly* the same probability while in the case of a shallow minimum the tunneling probabilities are *almost* the same. We will see below that the real time evolution of the fields after the tunneling leads to deviating bosonic signatures for two different trajectories. In any case, if a barrier penetration happens, both results occur (almost) equally likely, so that the accuracy of all results is given by the range of values which we obtain for different trajectories with the same action. Certainly, the tunneling rate is influenced by the volume of a possible transformation group with invariant action or the (low) curvature around the minimum, but these only contribute to the prefactor B of eq. (2.8) which is not discussed in this paper.

Thus, in Tab. 2 we have given both values for $N_{\rm CS}^{\rm esc}$ if we obtained two different configurations with the same action. We find that both the action and $N_{\rm CS}^{\rm esc}$ increase if $|\rho|$ is decreased or the Higgs mass ν is increased. The reason is that the barrier becomes wider and higher with decreasing $|\rho|$ and increasing ν so that more action is necessary to penetrate through it, and the escape point moves further away from the trivial vacuum. We see that both quantities are roughly linearly related to ρ, and, as anticipated, the dependence of the results on the Higgs mass is rather weak.

The suppression factor $e^{-2S_{\rm inst}} \approx 10^{-153}$ of the tunneling rate for $\rho = 0$ becomes less strong for $|\rho| > 0$, but significant tunneling amplitudes can only be obtained for chemical potentials as high as $|\rho| \gtrsim 0.9$ (for $\rho = -0.9$ and $\nu = 1$ we obtained $S_E/S_{\rm inst} = 0.06$ and $N_{\rm CS}^{\rm esc} = 0.17$). One needs, however, a matter density which is about 10^6 times larger than the photon density in the early universe at the electroweak phase transition, or about 10^{18} nuclear matter density, in order to correspond to such a large chemical potential. Presently it is not known if a matter density of this order has ever existed in the early universe. Even if this is not the case, our results still have some physical significance because the tunneling rate may be related to the rate of fermion number

violation at high particle energies [14]. Hence, taking our results one might be able to deduce the probability to observe such a process at a supercollider.

5.2 Real time evolution

Next we will describe how the system evolved in real time after the barrier penetration. We solved the equations of motion basically as it was done e.g. in [21, 22]. In order to check the numerics, we first used the sphaleron as starting configuration, and our results agreed with those of [21, 22]. Then we replaced the sphaleron by the configuration at the escape point of the barrier penetration process. By performing the gauge transformation with $\Delta N_{\rm CS} = -1$ to ensure that the fields fluctuate about the *trivial* vacuum (see Section 4) the potential energy of the starting configuration $V^{\mu}_{\rm pot}$ is increased from 0 to $|\mu|$ (in units of $\frac{8\pi^2}{g^2} m_W = \frac{\mu_{\rm crit}}{2}$ this means it is increased from 0 to $2|\rho|$). The Chern–Simons number is lowered by one unit and starts between -1 and 0.

In Fig. 4 we present the behavior of $V^{\mu}_{\rm pot}$, $T_{\rm kin}$, and $N_{\rm CS}$ as a function of time $t > 0$ after the tunneling process for $\rho = -0.6$ and $\rho = -0.9$. The Higgs mass is $\nu = 1$. We find that for times $t \lesssim 10$ the behavior of the system in the two cases is quite similar: The system starts to move, i.e. the kinetic energy increases, while the potential energy decreases. Energy conservation is fulfilled very accurately during the whole process. The Chern–Simons number increases quickly to values around 0, which means the systems comes close to the trivial vacuum.

In the case $\rho = -0.6$ the energy dissipates into small fluctuations about the vacuum. We checked that the energy $V^{\mu}_{\rm pot}{}^{(2)}$ in second order of the fluctuations agrees up to a deviation of less than 1% with $V^{\mu}_{\rm pot}$, moreover we see in Fig. 4 that potential and kinetic energy both become constant at the value of $\frac{|\mu|}{2}$ in accordance with the virial theorem. The Chern–Simons number takes a constant value slightly below zero. Hence the system has settled to small oscillations about the trivial vacuum and will stay in this topological sector forever (apart from possible tunneling later on). Later we will analyze the particle content of this state.

In the case $\rho = -0.9$, however, we observe a completely different behavior for times $t \gtrsim 10$. Here $N_{\rm CS}$ suddenly increases from values around 0 to about 1, later even to 2. Hence, the system does not stay in the topological sector of the trivial vacuum but moves classically over the next barrier to the sector with

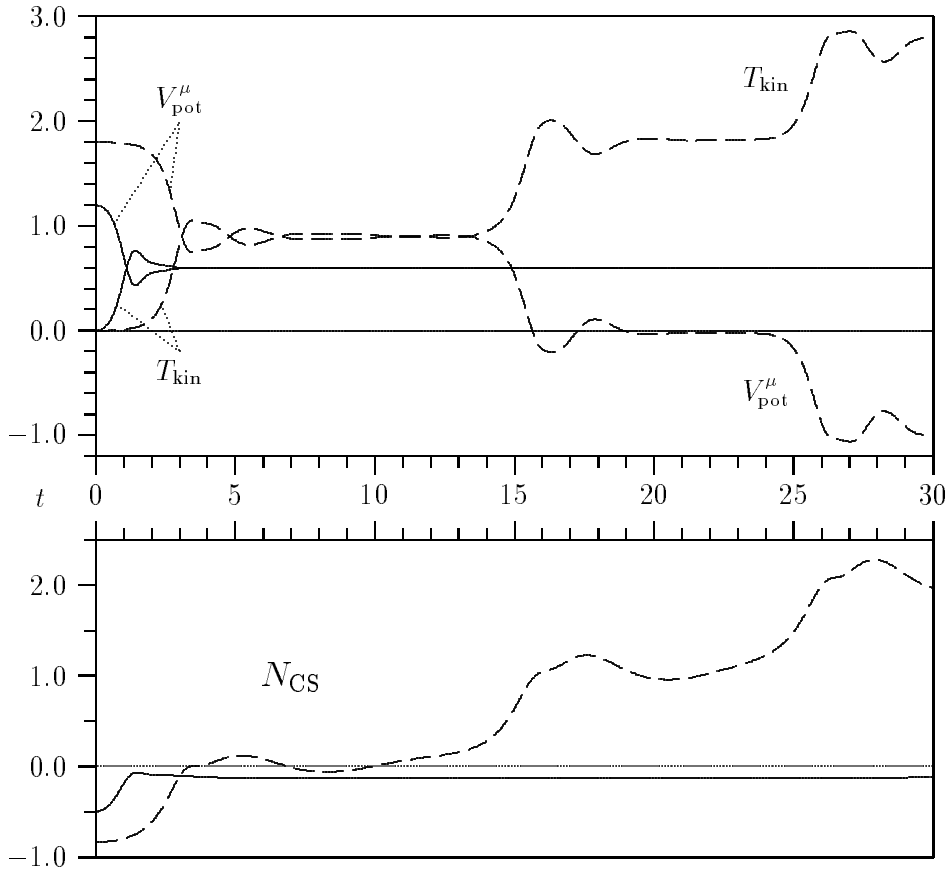

Fig. 4: The potential energy $V^{\mu}_{\rm pot}$, the kinetic energy $T_{\rm kin}$ (in units of $\frac{8\pi^2 m_W}{g^2}$), and the Chern–Simons number $N_{\rm CS}$ versus time t (in units of m_W^{-1}) for chemical potentials $\rho = \mu/\mu_{\rm crit} = -0.6$ (solid lines) and -0.9 (dashed lines), and the Higgs mass $\nu = m_H/m_W = 1$.

$N_{\rm CS} = 1$. Here it also stays only for a short period before it moves to the next sector with $N_{\rm CS} = 2$. This behavior is also demonstrated by the plot of the potential energy which shows the successive falls of the system like a cascade towards configurations with increasing winding number and decreasing energy. Once the first tunneling process has happened, the system moves classically over all the following barriers so that the whole fermion matter decays rapidly and sets free an enormous amount of energy. As mentioned above, the tunneling amplitude is not extremely small for $\rho = -0.9$ (10^{-9} instead of 10^{-153}), but in order to generate such a large chemical potential a huge fermion density is required ($\approx 10^{18}$ nuclear matter density).

It is a property of the periodic plus linear potential that even at small μ, the energy barriers become lower than the local minimum at $N_{\rm CS} = 0$, if one goes far enough in $N_{\rm CS}$. Therefore, if the systems tunnels directly to that far-away sector (which would require multi-instanton-like bounce solutions), the avalanche would probably develop, too. Of course, the multi-instanton tunneling probability is even smaller than for a single bounce, but it should grow faster with μ. It would be interesting to estimate the total decay probability as a function of μ, with tunneling to different topological sectors summed up.

Energetically, this behavior of a classical rapid decay is allowed if the top of the barrier between the sectors with $N_{\rm CS} = 0$ and 1 is lower than the chemical potential $|\mu|$. For $\nu = 1$, this is the case already for $|\rho| \gtrsim 0.2$, but we found that only for $|\rho| \gtrsim 0.9$ it actually happens. For chemical potentials between 0.2 and 0.9 the system could in principle cross the next barrier, but the energy is dissipated among the modes of small oscillations and not concentrated on the direction to the next minimum so that the system does not find the collective path over the barrier. For $\nu = 0$, we have found that the avalanche starts developing already at $|\rho| \gtrsim 0.8$. We think we have observed an interesting phenomenon of how an exponentially suppressed spontaneous decay triggers off a catastrophic avalanche which never stops until the fermion sea, originally filled up to the Fermi surface μ, is completely "splashed".

In Fig. 5 we show for $\nu = 1$ and $\rho = -0.6$ how the density of the total energy, defined by $E_{\rm tot} = T_{\rm kin} + V^{\mu}_{\rm pot} \equiv m_W \int_0^\infty dr\, e_{\rm tot}(r)$, evolves in time. Our plot is similar to the one given in [21, 22], where one starts with a slightly disturbed sphaleron instead of the configuration at the escape point of the bounce. As was found in [21, 22], the outgoing wave moves with almost the speed of light and shows some dispersion, but in our case the dispersion is less strong. For the sphaleron, after $t = 25\, m_W^{-1}$ the height of the pulse has decreased to about 30% of its original value at $t = 0$, while for the bounce configuration it drops only to about 65% of the value at $t = 0$.

Next we wish to analyze the particle content of the state after the tunneling. This is only possible if the system stays in the topological sector of the trivial vacuum and does not move classically over the next barrier. In this case after some time (typically $\sim 10\, m_W^{-1}$) the system has settled to small oscillations about the trivial vacuum so that one can perform the Fourier decomposition (4.8). Fig. 6 shows how the total energy ($= |\mu|$) is distributed among the Higgs and gauge boson modes. Integration of the curves yields the total energy of

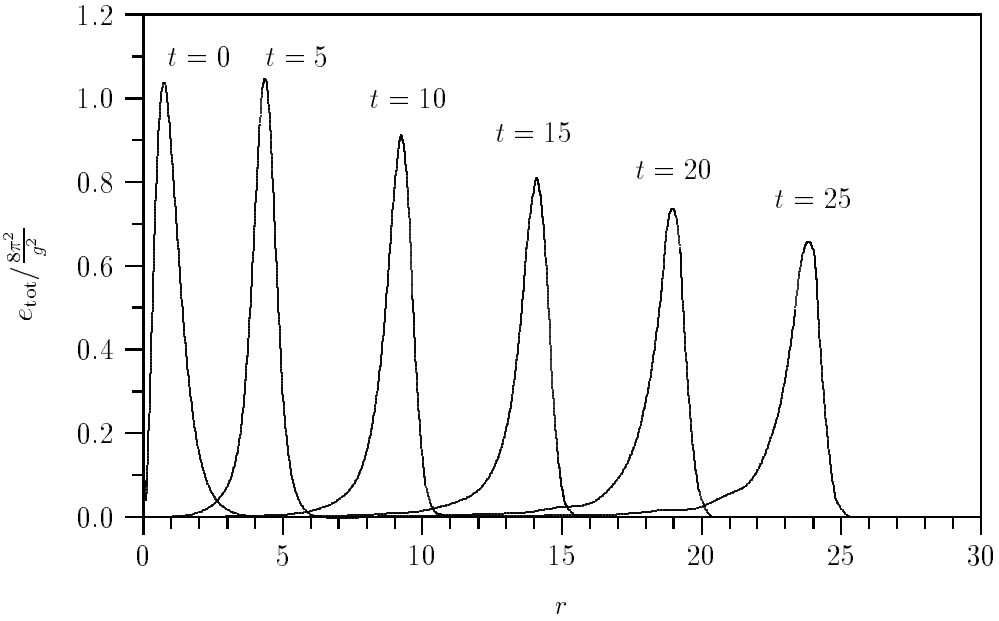

Fig. 5: The density $e_{\rm tot}$ of the total energy versus radial distance r for various times t (r and t in units of m_W^{-1}). The parameters are $\rho = \mu/\mu_{\rm crit} = -0.6$ and $\nu = m_H/m_W = 1$.

the Higgs (E_H) and gauge (E_W) bosons (see eq. (4.9)); we have found that the sum $E_H + E_W$ is equal to $|\mu|$ up to a deviation of usually less than 2%, which is another check of our numerics.

	$\rho = \mu/\mu_{\rm crit}$			
$\nu = \frac{m_H}{m_W}$	-0.2	-0.4	-0.6	-0.8
0	3.8/3.1[1)]	4.9/4.2[1)]	6.4/6.3[1)]	$--$[2)]
1	5.1	7.6	8.5	11.3
10	0.0	0.0	2.3	1.3/1.5[1)]

[1)] results of two different trajectories with the same action

[2)] system does not oscillate about trivial vacuum
but moves classically to next sector

Tab. 3: The ratio of the energy of the Higgs bosons to the total energy $E_H/(E_W + E_H)$ in percent after the system settles to small oscillations about the trivial vacuum. The results are given for various values of the chemical potential ρ and the Higgs mass ν.

In Tab. 3 we show how much of the energy is taken by the Higgs bosons (in percent). This number is generally in the range up to 10%; it increases slightly with $|\rho|$. If we increase the Higgs mass from $\nu = 0$ to $\nu = 1$ (and keep ρ fixed), the Higgs particles gain some energy on the expense of the gauge bosons, but for $\nu = 10$ the share of the Higgs bosons is almost zero. In this last case the Higgs bosons are too heavy to be produced at all, for small masses their total energy is basically correlated to the individual energy of each particle, i.e. it rises with the mass.

Fig. 6 demonstrates that the spectrum is shifted to larger k when ν is increased. This effect is particularly strong in the case of the Higgs bosons. For $\nu = 10$ the energy density takes its maximum at about $k \approx 5$ while for $\nu \lesssim 1$ it is only at $k \approx 1.5$, for $\nu = 0$ very light Higgs bosons with momenta around $k = 0$ are produced in a large number.

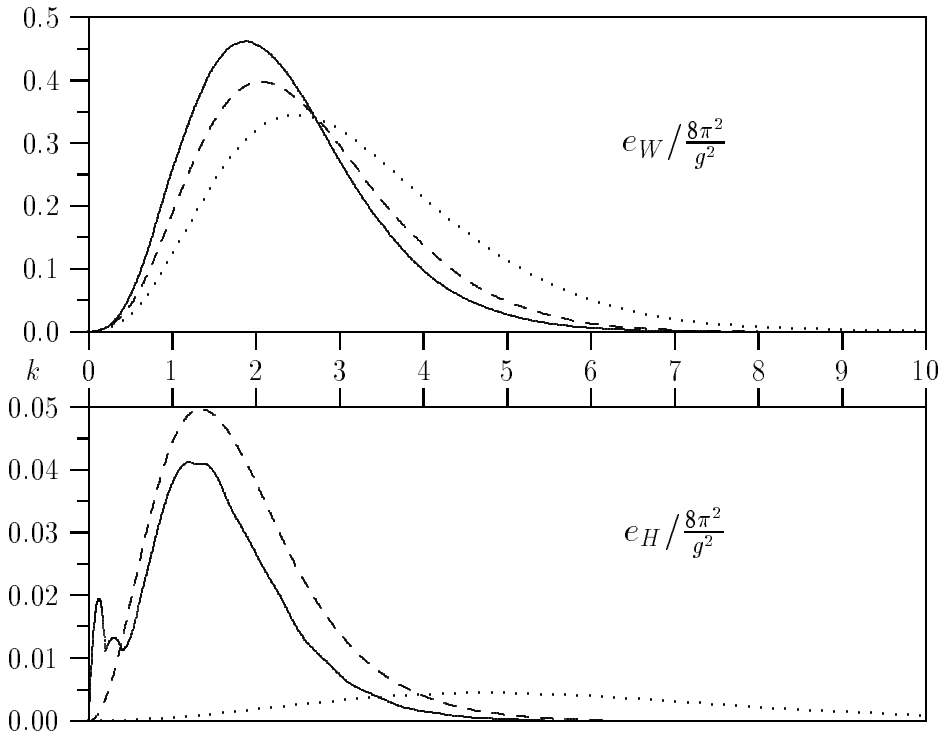

Fig. 6: The energy densities e_W and e_H of the gauge and Higgs bosons versus momentum k (in units of m_W) for Higgs masses $\nu = m_H/m_W = 0$ (solid lines), $\nu = 1$ (dashed lines), and $\nu = 10$ (dotted lines). The chemical potential is $\rho = -0.6$.

Tab. 4 shows the total particle numbers N_W and N_H of the gauge and Higgs bosons, respectively. In the case $\nu = 0$ the determination of N_H is not possible because the number density $n_H(k)$ is strongly peaked close to $k = 0$ so that the numerical error of the integration is uncontrollable. This is of course an artefact of the unphysical choice $\nu = 0$, however, also for finite, but small masses one would have to take many values in the k-lattice around 0 and perform the integration carefully to get a reasonable result. We find that the particle numbers rise with $|\rho|$, because the released energy increases and allows the production of more particles. The number of Higgs particles is much smaller than the number of gauge bosons, again we see that in case of a large Higgs mass no Higgs bosons are produced.

	$\rho = \mu/\mu_{\text{crit}}$			
$\nu = \frac{m_H}{m_W}$	-0.2	-0.4	-0.6	-0.8
0	24.5/22.7[1)] ––[2)]	49.0/45.5[1)] ––[2)]	74.2/69.3[1)] ––[2)]	––[3)] ––[3)]
1	22.9 1.9	46.2 5.9	67.1 9.6	102.6 16.8
10	20.8 0.0	40.3 0.0	64.3 0.4	117.2/112.4[1)] 0.3/0.4[1)]

[1)] results of two different trajectories with the same action

[2)] determination impossible due to infrared behavior

[3)] system does not oscillate about trivial vacuum
but moves classically to next sector

Tab. 4: The number of gauge bosons N_W (upper numbers) and Higgs bosons N_H (lower numbers) after the system settles to small oscillations about the trivial vacuum. The results are given for various values of the chemical potential ρ and the Higgs mass ν.

Finally we comment on the numerical uncertainty of the data in Tabs. 3 and 4. The error can be estimated by increasing the numerical parameters of the Runge–Kutta time integration and the number of k values in the Fourier transformation. Moreover one can choose different times t_{osc} (see explanation after eq. (4.8)) where we start to fit the amplitudes of the modes in momentum space. We find that the error of the data is in general less than 2%. We have

to keep in mind, however, that the bounce trajectory, and hence the starting configuration, is not unique, but in some cases there are different solutions with almost the same tunneling probability. These different starting configurations yield results for the particle content which can deviate up to 20%, as can be seen from the data in Tabs. 3 and 4. Therefore, the probability density for the particle content of the final state is spread over a range of numbers about $\pm 10\%$ around the value given in the tables.

6 Summary

In this work we have presented a method to find the bounce trajectory in the electroweak theory and calculated the probability for the decay of high density fermionic matter.

The bounce trajectory is obtained by minimization of the Euclidean action as a function of the discretized Higgs and gauge boson fields. At each step of the procedure the action is regarded as a function of only one parameter, i.e. it is minimized with respect to the value of one field profile function at a certain point in the lattice while the values of the other fields and at the other points are kept fixed. After finishing one step of the minimization one moves to the next field or next point until each field at each point of the lattice has been considered. Many of such "sweeps" through the lattice (of the order of 10000) have to be performed until a stable configuration is reached which does not change any more if it undergoes further sweeps. From time to time the user has to interfere into the process of minimization. The program contains several options to manipulate the field configuration, partially in order to keep the fields in a continuous and smooth shape, partially in order to accelerate the convergence. It has been checked that the final configuration always fulfills the Euclidean equations of motion with sufficient accuracy.

The determination of the bounce has been carried out for several choices of the Higgs mass $\nu = m_H/m_W$ and the chemical potential $\rho = \mu/\mu_{\rm crit}$ of the fermionic matter. We find that the action S_E of the bounce drops from the instanton action $S_{\rm inst}$ at $\rho = 0$ to zero at $|\rho| = 1$ roughly linearly and depends only weakly on ν. A similar behavior is found for the Chern–Simons number of the escape point of the bounce, $N_{\rm CS}^{\rm esc}$, which decreases from 1 to 0. The action S_E is the exponent of the tunneling rate which itself is correlated to the probability of the fermion number violation at high particle energies. It might

therefore be possible to use our results for S_E in order to predict the cross section of the high energy process.

For several sets of parameters we found that the bounce solution is not unique; instead there exist several solutions with different escape points, but with the same action (in the given frame of accuracy). Since after the barrier penetration each of these escape points will be taken with the same probability, for some results of this work we can only give a range of values instead of a definite number.

After the tunneling process, the bosonic fields can evolve in real time Minkowskian space since they have obtained the energy of the annihilated fermions as potential energy. The equations of motion can here be solved by some time integration method rather than a minimization of the action.

For chemical potentials $|\rho| \lesssim 0.8$ the system stays in the topological sector where it came to after the tunneling and settles to small oscillations about the minimum. The oscillations correspond to the radiation of the Higgs and gauge bosons, and we have analyzed the particle content of this state by Fourier transformation. We find that usually less than 10% of the energy is absorbed by the creation of the Higgs bosons, and correspondingly the total number of produced gauge bosons is also about 10 times greater than the number of Higgs bosons. The results depend strongly on ρ and partially also on the Higgs mass ν. For large chemical potentials $|\rho| \gtrsim 0.9$ the system has enough energy and coherence after the tunneling to move classically over the next barriers. This corresponds to an avalanche decay of the fermionic matter and to the production of an enormous amount of Higgs and gauge bosons.

Acknowledgements: We are grateful to C.Weiss for pointing our attention to the use of relaxation methods ([16]), and thank P.Pobylitsa, M.Polyakov, and V.Petrov for numerous discussions. The work has been supported in part by the Deutsche Forschungsgemeinschaft and the RFBR grant 95-07-03662.

Appendix

To investigate the real time behavior after tunneling one only needs the field configuration at the escape point of the bounce (which we fix at $t = 0$) rather than the functions $A(t, r)$, ..., $G(t, r)$ in the whole two-dimensional space t, r. Hence it is useful to have a parameterization of the functions $A(0, r)$, ..., $G(0, r)$ so that one can take them as input for further calculations without having the necessity to recalculate the complete bounce trajectory. In this appendix we give an analytic fit which matches the numerically determined functions $A(0, r)$, ..., $G(0, r)$ very accurately. The potential energy and the Chern–Simons number of the fit agree with the corresponding values of the numerical configuration up to a deviation of about 1%. Following the real time behavior of the fit and the numerical fields we find that the particle numbers N_W, N_H and the energies E_W, E_H are reproduced up to a deviation less than 3%.

The parameterization is chosen so that it includes the possibility to describe both the trivial vacuum with $N_{\rm CS} = 0$ and the non-trivial vacuum with $N_{\rm CS} = 1$. For this reason the fit is performed in a gauge where the field $D(r) \equiv 0$ everywhere. We denote the other fields in this gauge by $A_0(r)$, $B_0(r)$, $H_0(r)$, $G_0(r)$. (Here and in the following the argument $t = 0$ is dropped.) The gauge transformation which transforms $A_0(r)$, ..., $G_0(r)$ to the field configuration $A(r)$, ..., $G(r)$ at the escape point of the bounce is described by some function $P(r)$ according to eq. (2.12).

For the functions $P(r)$, $D(r)$, $A_0(r)$, $B_0(r)$, $H_0(r)$, $G_0(r)$ we use the following ansatz:

$$\begin{aligned}
P(r) &= -\lambda_d\Big[d_0\Big(1+\tfrac{r}{2\lambda_d}\Big) + d_2\Big(1+\tfrac{r}{\lambda_d}+\tfrac{r^2}{2\lambda_d^2}\Big) \\
&\qquad\qquad + 3d_3\Big(1+\tfrac{r}{\lambda_d}+\tfrac{r^2}{2\lambda_d^2}+\tfrac{r^3}{6\lambda_d^3}\Big)\Big]e^{-r/\lambda_d}\,, \\
D(r) &= 2P'(r) = \Big[d_0\Big(1+\tfrac{r}{\lambda_d}\Big) + d_2\tfrac{r^2}{\lambda_d^2} + d_3\tfrac{r^3}{\lambda_d^3}\Big]e^{-r/\lambda_d}\,, \\
A_0(r) &= a_0\Big(1+\tfrac{r}{\lambda_a}+a_2\tfrac{r^2}{\lambda_a^2}+a_3\tfrac{r^3}{\lambda_a^3}\Big)e^{-r/\lambda_a}+1\,, \\
B_0(r) &= b_0\Big(1+\tfrac{r}{\lambda_b}+b_2\tfrac{r^2}{\lambda_b^2}+b_3\tfrac{r^3}{\lambda_b^3}\Big)e^{-r/\lambda_b}\,, \\
H_0(r) &= \Big[h_0\Big(1+\tfrac{r}{\lambda_h}\Big) + h_1 r + h_2\tfrac{r^2}{\lambda_h^2} + h_3\tfrac{r^3}{\lambda_h^3}\Big]e^{-r/\lambda_h}+1\,, \\
G_0(r) &= \Big[g_0\Big(1+\tfrac{r}{\lambda_g}\Big) + g_1 r + g_2\tfrac{r^2}{\lambda_g^2} + g_3\tfrac{r^3}{\lambda_g^3} + g_4\tfrac{r^4}{\lambda_g^4}\Big]e^{-r/\lambda_g}\,. \qquad \text{(A.1)}
\end{aligned}$$

The procedure how we obtain the parameters in eq. (A.1) is the following: To

ensure the correct behavior of the fitting functions at $r = 0$ (eq. (2.13)) we first take $d_0 = B'(0)$ (evaluated by a quadratic fit of B at $r = 0$), use a suitable fitting algorithm for $D(r)$ to determine λ_d, d_2, and d_3, and set

$$\begin{aligned}
a_0 &= \cos\Big(2\lambda_d(d_0 + d_2 + 3d_3)\Big) - 1\,, \\
b_0 &= \sin\Big(2\lambda_d(d_0 + d_2 + 3d_3)\Big)\,, \\
h_0 &= H(0)\cos\Big(\lambda_d(d_0 + d_2 + 3d_3)\Big) - 1\,, \\
g_0 &= H(0)\sin\Big(\lambda_d(d_0 + d_2 + 3d_3)\Big)\,, \\
h_1 &= \Big(H(0)\tfrac{d_0}{2} - G'(0)\Big)\sin\Big(\lambda_d(d_0 + d_2 + 3d_3)\Big)\,, \\
g_1 &= -\Big(H(0)\tfrac{d_0}{2} - G'(0)\Big)\cos\Big(\lambda_d(d_0 + d_2 + 3d_3)\Big)\,,
\end{aligned} \tag{A.2}$$

where we have used $P(0) = -\lambda_d(d_0 + d_2 + 3d_3)$. The parameters λ_a, λ_b, λ_h, λ_g, are held fixed:

$$\lambda_a = \lambda_b = 0.8\,, \qquad\qquad \lambda_h = \lambda_g = 0.6\,. \tag{A.3}$$

Then we perform a gauge transformation on the fields $A(r), \ldots, G(r)$, using the function $P(r)$ of eq. (A.1) to obtain $A_0(r), \ldots, G_0(r)$. These functions are fitted to yield the remaining parameters a_2, a_3, b_2, b_3, h_2, h_3, g_2, g_3, and g_4. Altogether, our fits contain 12 parameters determined by the fitting algorithm plus 7 parameters depending on the three values $B'(0)$, $H(0)$, and $G'(0)$. So in total the number of free parameters is 15.

In Table 5 the results of the parameters are given for several values of the chemical potential ρ and the fixed Higgs mass $\nu = m_H/m_W = 1$. For this Higgs mass we always obtain a unique field configuration at the escape point, i.e. it does not depend on the initial configuration before the minimization of the action starts.

$\rho = \mu/\mu_{\rm crit}$	-0.2	-0.4	-0.6	-0.8	-0.9
a_0	-1.166	-1.873	-1.957	-1.379	-0.685
a_2	-0.123	-0.183	-0.108	$+0.358$	$+1.100$
a_3	-0.042	-0.006	-0.020	-0.084	-0.144
b_0	$+0.986$	$+0.487$	-0.290	-0.925	-0.949
b_2	-0.738	-0.472	-1.008	-0.138	$+0.326$
b_3	$+0.180$	$+0.270$	-0.303	-0.224	-0.349
λ_d	$+0.258$	$+0.320$	$+0.343$	$+0.528$	$+0.705$
d_0	-5.514	-3.165	-2.224	-1.001	-0.501
d_2	-3.298	-2.524	-1.926	-1.341	-0.740
d_3	$+0.001$	-0.005	$+0.000$	$+0.162$	$+0.118$
h_0	-0.674	-0.976	-0.957	-0.625	-0.299
h_1	$+0.663$	$+0.974$	$+0.963$	$+0.538$	$+0.228$
h_2	$+0.153$	$+0.129$	$+0.118$	$+0.031$	-0.011
h_3	-0.025	-0.016	-0.015	-0.005	$+0.000$
g_0	$+0.389$	$+0.092$	-0.285	-0.561	-0.506
g_1	-0.556	-0.254	$+0.145$	$+0.360$	$+0.315$
g_2	-0.141	-0.104	-0.043	$+0.009$	$+0.011$
g_3	$+0.134$	$+0.117$	$+0.066$	-0.027	-0.057
g_4	-0.019	-0.013	-0.004	$+0.010$	$+0.018$

Tab. 5: The parameters of the fitting functions for the configuration at the escape point of the bounce trajectory according to eq. (A.1) for several values of the chemical potential ρ and the Higgs mass $\nu = m_H/m_W = 1$.

References

[1] G.'t Hooft, *Phys. Rev. Lett.* **37**, 8 (1976).

[2] L.D.Faddeev, in *Proceedings of the IVth International Conference on Nonlocal Field Theories*, Dubna, USSR, 1976 (Joint Institute for Nuclear Research, Dubna, 1976).

[3] R.Jackiw and C.Rebbi, *Phys. Rev. Lett.* **37**, 172 (1976).

[4] R.Dashen, B.Hasslacher, and A.Neveu, *Phys. Rev.* **D10**, 4138 (1974).

[5] N.Manton, *Phys. Rev.*, **D28**, 2019 (1983);
F.R.Klinkhamer and N.S.Manton, *ibid.* **30**, 2212 (1984).

[6] V.Kuzmin, V.Rubakov, and M.Shaposhnikov, *Phys. Lett.* **B155**, 36 (1985); **B191**, 171 (1987).

[7] P.Arnold and L.McLerran, *Phys. Rev.* **D36**, 581 (1987); **37**, 1020 (1988).

[8] D.Diakonov, M.Polyakov, P.Sieber, J.Schaldach, and K.Goeke, *Preprint* RUB-TPII-25/95, hep-ph/9502245, to be published in *Phys. Rev.* **D**.

[9] A.Ringwald, *Nucl. Phys.* **B330**, 1 (1990).

[10] O.Espinosa, *Nucl. Phys.* **B334**, 310 (1990).

[11] L.McLerran, A.Vainshtein, and M.B.Voloshin, *Phys. Rev.* **D42**, 171 (1990).

[12] M.P.Mattis, *Phys. Rep.* **214**, No.3 159 (1992).

[13] V.Rubakov and A.Tavkhelidze, *Phys. Lett.* **B165**, 109 (1985);
V.Rubakov, *Prog. Theor. Phys.* **75**, 366 (1986);
V.Matveev, V.Rubakov, A.Tavkhelidze, and V.Tokarev, *Nucl. Phys.* **B282**, 700 (1987).

[14] D.Diakonov and V.Petrov, *Phys. Lett.* **275B**, 459 (1992).

[15] S.Coleman, *Phys. Rev.* **D15**, 2929 (1977);
C.G.Callan, S.Coleman, *Phys. Rev.* **D16**, 1762 (1977).

[16] S.L.Adler and T.Piran, *Rev. of Mod. Phys.* **56**, 1 (1984).

[17] V.A.Rubakov, B.E.Stern, and P.G.Tinyakov, *Phys. Lett.* **B160**, 292 (1985).

[18] Y.Kobayashi, *Prog. Theor. Phys.* **90** 885 (1993).

[19] A.Kusenko, *Phys. Lett.* **B358**, 51 (1995).

[20] J.Schaldach, P.Sieber, D.Diakonov, and K.Goeke, *Preprint* RUB-TPII-28/95, hep-ph/9601245, to be published in *Phys. Lett.* **B**.

[21] M.Hellmund and J.Kripfganz, *Nucl. Phys.* **B373**, 749 (1991).

[22] W.N.Cottingham and N.Hasan, *Nucl. Phys.* **B392**, 39 (1993).

[23] T.Akiba, H.Kikuchi, and T.Yanagida, *Phys. Rev.* **D38**, 1937 (1988).

[24] D.Diakonov, M.Polyakov, P.Sieber, J.Schaldach, and K.Goeke, *Phys. Rev.* **D49**, 6864 (1994).

[25] I.Affleck, *Nucl. Phys.* **B191**, 429 (1981).